A Search for Gravitational Wave Transients from Core Collapse Supernovae Using the Coherent WaveBurst Search Algorithm

Alexander Adams Corpuz*

Embry-Riddle Aeronautical University,

3700 Willow Creek Rd, Prescott, AZ 86301, USA.

(ΩDated: March 9, 2010)

Abstract

In an effort to detect gravitational waves, an international collaboration has implemented a network of laser interferometers. One way to analyze the raw data produced by these detectors is to employ a coherent analysis program known as coherent WaveBurst (cWB). In our search for signals from core-collapse supernovae in S6, the algorithm identifies triple coincidence triggers. By injecting numerical and analytic supernova waveforms into the data stream we are able to test the network and algorithm efficiency. By carefully tuning the search parameters, we have been able to increase our efficiency values by a minimum factor of two in the past 2 months. We can dan state our results with a degree of confidence based on our false alarm rate which depends on which tuning is being implemented. This is an ongoing search that has not yet fully matured.

* corpuza@erau.edu

I. THEORY

The theory of General Relativity predicts that quadrupole and higher mass motions will radiate energy in the form of gravitational waves (GW). GW are perturbations of the space-time metric generated by said motions. There exist many different theoretical models capable of producing gravitational waves. These include astrophysical phenomena such as gamma ray bursts, black hole interaction and coalescences, neutron star coalescence, pulsar glitches, and core-collapse supernovae (CCSN). CCSN are particularly interesting sources as their gravitational emission can reveal important dynamics of stellar interiors than can be observed in no other way [1]. The exact trigger mechanism that causes core-collapse is unknown, as is the precise nuclear equation of state of hot nuclear matter. Both of these unknown aspects of stellar objects can be revealed through the detection and analysis of the associated GW.

II. GRAVITATIONAL WAVE EMISSION WAVEFORMS

There are several mechanisms theorized to cause gravitational wave emission in a CCSN. The three used to generate waveforms for this analysis are convection and standing accretion shock instability (SASI), proto-neutron star (PNS) g-modes, and analytic models. Models focusing on PNS g-modes have not yet been implemented in our search, but will be included further on.

Convection and SASI are two different GW producing mechanisms present in CCSN. They are grouped together because they occur in the same spacial domain, and SASI-related distortions at significant amplitudes dynamically modify convection by distorting the post-shock region. Because of this, the GW signals of these hydrodynamic instabilities cannot be cleanly separated in supernova simulations [2].

A. Convection/SASI

As a stars's core exceeds it's Chandrasekhar mass, it grows gravitationally unstable and begins to collapse. Stellar matter falls inward condensing the core into a PNS. When in-

[1] For the complete list of waveforms implemented thus far, see Table 2 and 3

falling matter hits the PNS it bounces generating a hydrodynamic shock wave outward. As the post-bounce matter wave hits the in-flowing matter, the shock is stalled. The stalling bounce shock produces an negative entropy gradient in its wake. Bursts of electron neutrinos generate a negative lepton gradient. Together, these create a convectively unstable region. The resulting convective motion is known as prompt convection. The negative lepton gradient also stimulates whats is called PNS convection. In this process, the PNS contracts as it deleptonizes after the explosion. Neutrino heating below the stalled shock region creates a negative entropy gradient that again makes the convective region unstable. The resulting convective overturn is known as neutrino driven convection. In this type of convective motion, the SASI become a key factor in the GW emission. [2]

The studies performed by Ott et al. 2009 [3] contain signals generated by all three forms of convection. Marek et al. 2009 [4] waveforms have prompt convection and neutrino driven convection/SASI. The Marek2009 waveforms are the result of studying the GW waveform dependence on the nuclear equation of state (EoS), primarily the Lattimer-Swesty and Wolff EoS. Kotake et al. 2009 [5] waveforms are the result of neutrino driven convection/SASI focussing mainly on the contribution made by the SASI. Scheidegger et al. 2010 [6] includes waveforms from non- and slowly rotating models GW emission from to prompt- and lepton driven convection. This effort focussed on discovering details about the hydrodynamical state of the fluid inside the PNS. The study performed by Yakunin et al. 2010 [7] GW emission is from PNS and neutrino driven convection/SASI. It is important to add that these are all 2 dimensional models with the exception of Kotake et al. 2009.

B. Analytic Models

Fryer et al. 2007 [8] investigated the bar-mode instabilities of accretion induced collapse (AIC). Most CCSN models are unstable to bar-mode instabilities, however, an AIC is not. The parameters that define the bar-mode models are mass (0.2 and 1.5 $m_{\odot}$), frequency (200 and 1000Hz), and duration (100ms and 1s).

Piro et al. 2002 [9] investigate collapsar disk fragmentation. A failed supernova that collapses into a back hole will form an accretion disk of the remaining stellar material. The disk fragments into gravitationally bound clumps that then rotate rapidly around the black hole before being disrupted. These generate a unique gravitational wave signature not unlike

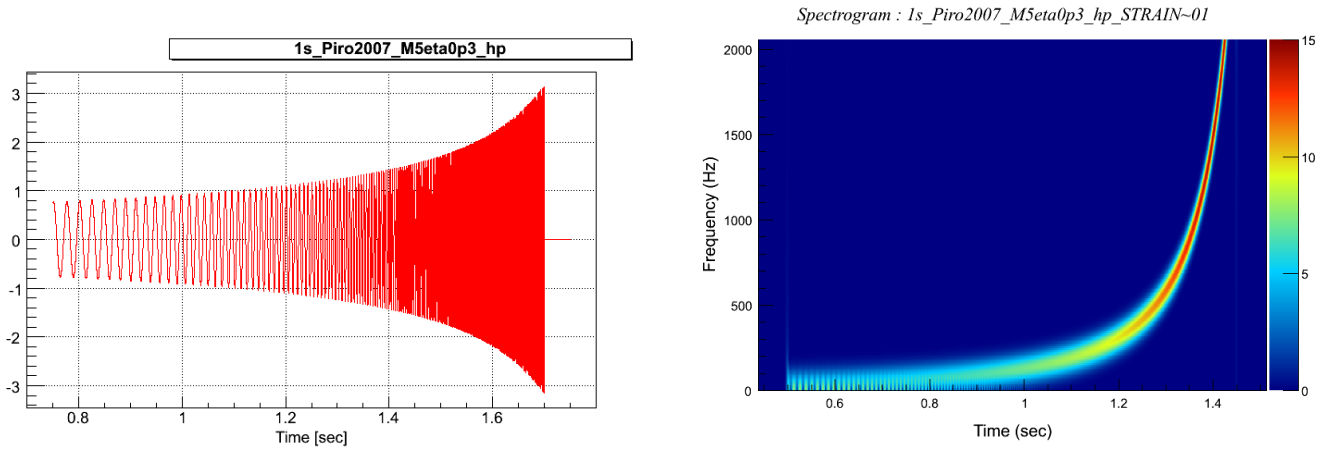

FIG. 1: Piro2007_M5eta0.3 h_+ polarization waveform (left) Corresponding waveform spectrogram (right)

a chirp signal. See Figure 1

III. COHERENT WAVEBURST SEARCH ALGORITHM

In the search for GW, there are two ways to combine data from multiple detectors: incoherently and coherently. Incoherent analysis pipelines generate potential GW triggers for individual detectors separate from the network and assume individual detector events to be network events. Coherent analysis pipelines generate GW triggers from a set of data from several detectors. Coherent analysis allows for waveform reconstruction and a higher direction reconstruction precision than incoherent analyses with multiple detectors.

GW Burst searches are based on the estimation of a detection confidence for a given false alarm rate (FAR). This is done by characterizing detection efficiencies and estimation of the background. Detector efficiencies are measured through simulated injections. Signal waveforms are injected into the data stream adding to the data's noise amplitude and an algorithm counts how many of the injected signals are detected. Typically, this is done with gaussians and sine-gaussians as they have a large bandwidth which provides better analytical results. For CCSN, there are a great number of waveforms generated by numerical simulations done in both two and three dimensions. For this search, we chose to implement both numerical and analytic waveforms. A quantity known as "h_{rss}" is used to characterize

the injected signal as it directly relates to GW signal energy [10]

$$h_{rss} = \sqrt{\int_{-\infty}^{\infty} h(t)^2 dt} \tag{1}$$

The majority of the waveforms implemented were given in terms of h_{rss} from a source fixed at 10kpc. Some of the waveforms however, the Ott et al. 2010 and Marek et al. 2009, were given in centimeters as the amplitude of the mass quadrupole moment at the source. These were scaled for detection range estimation using the "2, 0" quadrupole factor and a distance factor of:

$$\sqrt{\frac{\frac{15}{\pi}}{8}} \frac{1}{10kpc} \tag{2}$$

IV. PROCEDURE

The plan for this search was to modify the cWB all-sky search approach by implementing a celestial skymask. In the typical all-sky approach, the search algorithm will search for transient events across the entire sky and throughout the whole length of the data set (in the case of LIGO's S6 science run, this is split into S6a, S6b, S6c, and S6d). Through the implementation of a skymask, we limit the data that is processed to only that which corresponds with a given celestial position. We also place a constraint on the time window to be analyzed to correspond to the uncertainty window around one of our optical supernova targets. For our purposes, we have selected a skymask consisting of 3 pixels with dimensions 0.4° x 0.4°. We have generalized our time window to be ±5.5 days from our source time. Electromagnetic (EM) emission from a SN can take from a few seconds to several hours to escape a star. Those first EM signatures are first seen between seconds and weeks from the time of collapse. Using a light curve, it is possible to determine the approximate time of the actual explosion giving a case-by-case uncertainty in GW emission time [11]. Of the uncertainties that have currently been calculated for S5 events, ±5.5 days encompasses them all.

For our initial test purposes we have selected supernova 2009ib as our test case. We have selected it for several reasons. First, the supernova was first detected in the S6a segment. This is by far the best segment of time in the LIGO S6 run. Later segments have much more

[1] For a complete list of optically discovered targets within 20Mpc during S6a, see Table 4

fragmented data. Also, S6d has several issues with VIRGO at low frequencies. The second reason we selected this event was because it was a type-IIp supernova. The light-curves for type-IIp supernovae are very well known and can be used to more accurately narrow the time uncertainty. The third reason is proximity. It is the closest type-IIp supernovae that fits the previous two criterion.

In the following subsections, I will elaborate on several of the elements of this search

A. Background Studies

Our search begins with a quick check of our proposed method, that is, the modification of the cWB all-sky approach using a celestial skymask. The point of implementing a skymask is not only to reduce computational time, but also to reduce the false alarm rate (FAR), the rate at which the algorithm detects triple coincidence triggers that survive all the threshold cuts, to make any surviving events from our final search more statistically significant.

To cross check our method, we perform a series of background studies to ensure we get a significant FAR reduction. We perform a series of time lags in which our reference interferometer (in this case L1) is shifted in time by 1s. The interval of 1s is to ensure that no actual gravitational wave signals will contribute to the background triggers. As the maximum light travel time between the L1H1V1 network detectors is 27ms, 1s is more than sufficient to be sure that no triple-coincidence events present in the zero lag (no time shift) survive to add to the background.These time shifts of the L1 detector data are circular within the segment and are performed 201 times. These shifts of an 11 day period provide us with the equivalent of 6 years of background noise. The result is an average of background triggers for a given tuning.

Currently we are implementing 2 different tunings of the false alarm rate. The first is a much stricter tuning while the second is a more relaxed cut. The factors we manipulate in order to tune the FAR are the effective correlated SNR(ρ), the network correlation coefficient (cc), the black pixel probability (bpp), and the low frequency threshold. The values for both our hard tuning and soft tuning parameters can be seen in Table 1.

TABLE I: Hard and Loosened Tuning Parameters

Parameter	Hard Tuning	Loosened Tuning
$\rho > \rho_{thresh}$	3.2	2.5
cc $>$ cc$_{thresh}$	0.5	0.3
bpp $>$ bpp$_{thresh}$	0.0005	0.005
freq $>$ freq$_{thresh}$	100Hz	64Hz
freq $<$ freq$_{thresh}$	2048Hz	

The effective correlated SNR is defined as follows:

$$\rho = \sqrt{\frac{e_c}{N} cc} \tag{3}$$

Where cc is the network correlation coefficient defined by the *correlated energy* E_c and the *null energy* N_{ull} in Equation 4

$$cc = \frac{E_c}{E_c + N_{ull}} \tag{4}$$

and e_c is the *reduced correlated energy* defined by the Likelihood in matrix form and the *Pearson's correlation coefficient*, r_{mn}

$$e_c = \sum_{m \neq n} L_{mn} |r_{mn}| \tag{5}$$

The black pixel probability is the probability that a pixel with significant energy and no other pixels around it will be selected as a background trigger. The low frequency threshold is simply the lowest frequency at which a triple coincidence event can be considered a trigger.

From this cross check, we can clearly see a significant reduction in the false-alarm rate in Figure 2. The all-sky method has a FAR of 3e-4. Our hard tuning has a FAR 8e-6. The loosened tuning (not displayed here) has a FAR of 2e-6. Our desired target is 1e-6 as this will mean we will find about 31 events per year. While this is quite high, we will be able to use any false alarms to further fine-tune our search or identify interesting events.

In Figure 3, we can see the reduction of triple-coincidence events, especially at higher frequencies where most of our waveforms have the majority of their energy.

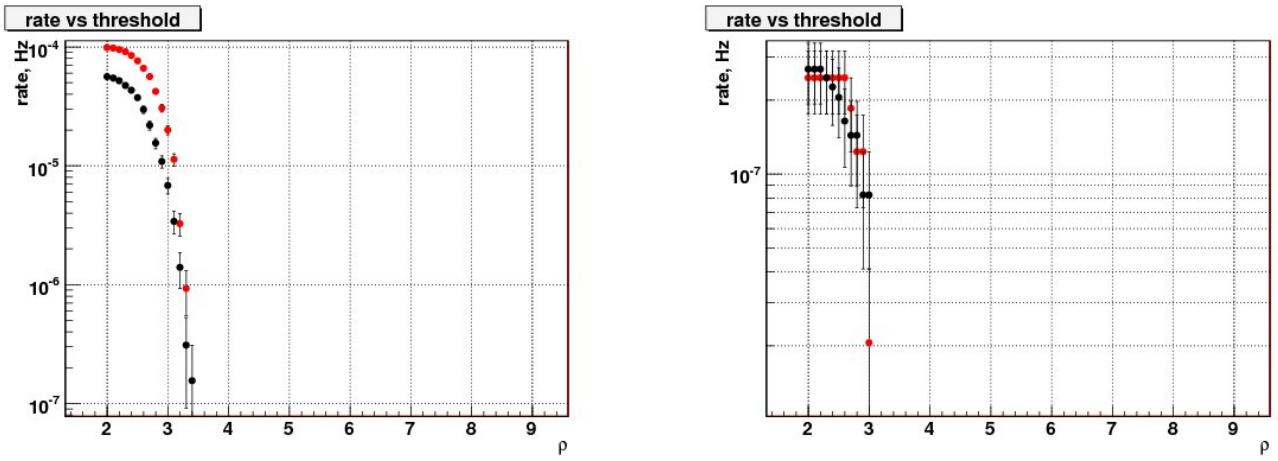

FIG. 2: (left) FAR for an all-sky search. (right) FAR for a search using a celestial skymask and the higher tuning. Note: Black is for <200Hz and Red is >200Hz

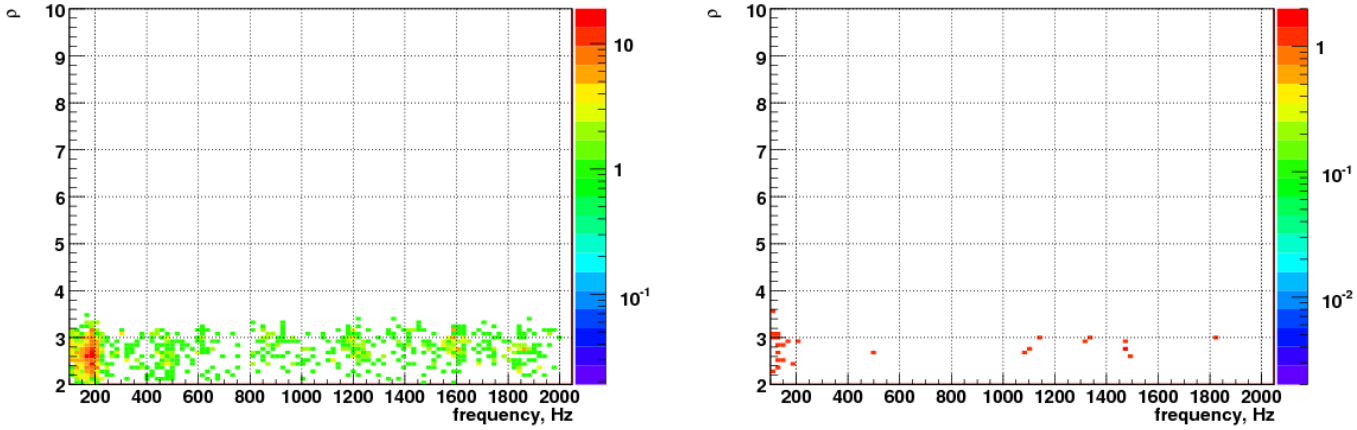

FIG. 3: (left) Trigger density of the all-sky simulation as a function of frequency and ρ (right) Same, but for a simulation implementing a skymask

B. Mock Data Challenge

The Mock Data Challenge, (MDC), is a common method within the GW community for injecting simulated waveform data into the data stream from the detectors. Before we could generate a set of injections, we implemented a standardization of the all the waveforms that we intended to used. We began by resampling each waveform at 16384Hz. Each waveform was padded to the nearest 1/4 second with zeros. We were also forced to truncate the

Piro waveforms at about only the last 1s of its duration. After analyzing the spectrograms, we concluded that most of the energy in the waveforms is present in the last second and energy before that is too low frequency to detect. This was done because cWB has some complicated issues with waveforms that are of a duration of much more than 1s.

MDC sets are produced by the Burst-MDC software package developed in the LIGO group [12]. This software package takes a set of input waveforms and prepares data stream injections at intervals of 100s. These signals are injected at a fixed h_{rss}, 2.5e-21 from a fixed sky location consistent with out test supernova, 2009ib. The Burst-MDC package also uniformly randomizes the polarization angle, psi. Because these signals are injected from a given direction, they reach the detectors at different times and each detector picks up different combinations of plus and cross components due to the different orientation of their arms.

C. Simulations

The simulation stage of our analysis consists of introducing the MDC into the data stream and feeding it into our analysis pipeline. The purpose of these simulations is to test the limits of the detectors and the cWB algorithm in the context of realistic supernova waveforms. Each injection is scaled using a series of strain factors which act on the h_{rss} of the waveform. These factors are 0.1, 0.2, 0.4, 0.8, 1.6, etc. Therefore, from our injected h_{rss} of 2.5e-21, we get injections at intervals appropriate for a logarithmic scale (2.5e-22, 5e-22, 1e-21, 2e-21, 4e-21, ...) The exact strain factors used for each waveform vary as the pipeline sensitivity varies depending on the waveform. The more strain factors used, the longer the computation time, although there is an average of 8 strain factors per simulation. Using these scaled injections, we can generate detector efficiency plots. These are counting experiments that tell us what percentage of injections we would expect to detect if the injected waveform had a given amplitude. These are very useful because they tell us how far we would expect to be able to detect a supernovae if it had a particular waveform. For a sample of an efficiency plot, see Figure 5.

One of the first problem to arise with our simulations was an anomalous transient event seen in the coherent event display (CED) reconstruction of the injected waveform. We discovered that our waveform resampling introduced a high-frequency transient into several

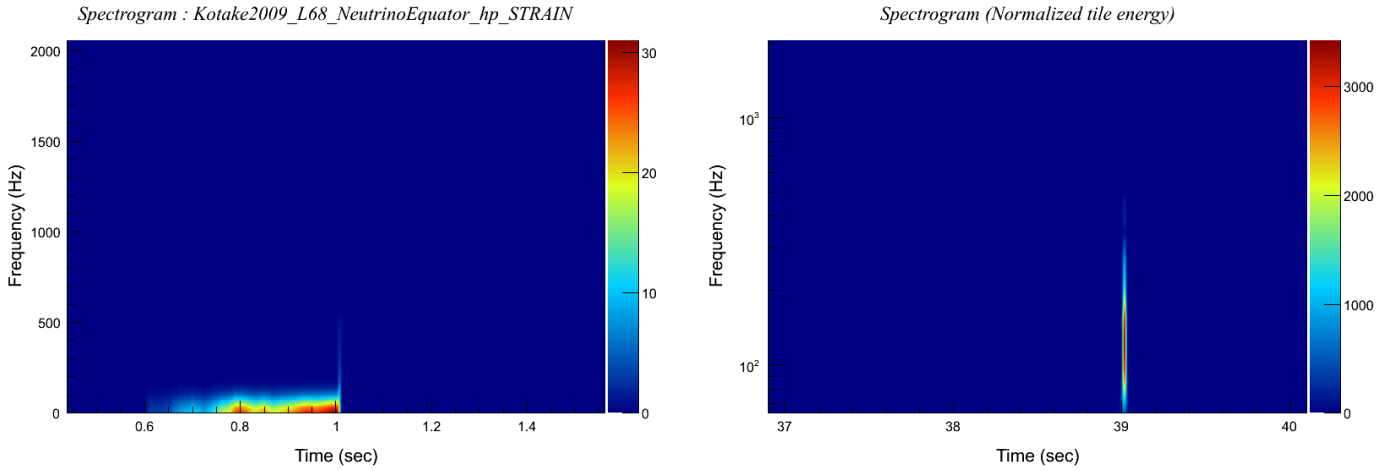

FIG. 4: A neutrino waveform spectrogram with the artificial transient (Left) The spectrogram of the same reconstructed waveform from the detected signal (right)

of our waveforms that needed to be dealt with. See Figure 4. From the spectrogram and waveform, we can see that the high-frequency event being detected is NOT part of the original waveform. This addition was due to the fact that the waveform files end at an amplitude greater than zero. When the waveform file ended, our resampled waveform went to zero at a much higher frequency than the rest of the waveform. This problem was solved with a low amplitude ring-down at the initial sampling frequency in which the waveform was obtained. This effectively eliminated the transient without adding any significant energy to the signal. Upon re-running those simulations, we found this artificial transient was the only portion of our neutrino generated waveforms that could be detected by our algorithm as most of their energy resides at frequencies below our low frequency threshold. Because of this, we decided to eliminate the neutrino waveforms from our search. This decision was confirmed by the parallel effort at CalTech using the x-pipeline algorithm.

The next issue to arise was a severe fragmentation of our selected window. We had initially believed that because we has selected a window within S6a, that fragmentation would be minimal. As it turns out, once category 2 disqualifications were applied, our test window of 2 days was reduced to 0.44 days. only 22% of our initial window. All of our collected data on network efficiencies needed to be scrapped at this point as none of the resulting efficiencies were statistically significant, although we had the advantage of knowing what the issues were with particular waveforms and how to solve them in the context of the

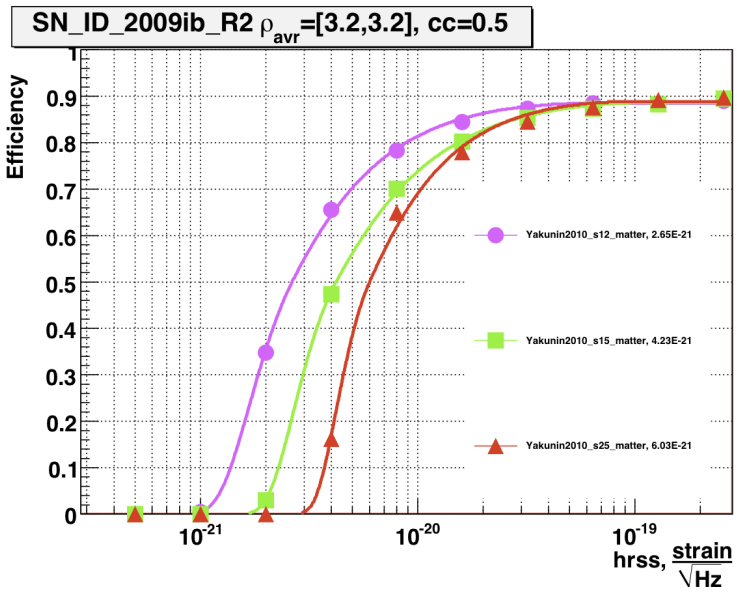

FIG. 5: Yakunin et al. 2010 waveform high threshold efficiencies

search as a whole. So we have since proceeded in running our initially intended 11 day time window with results for our harder tunings with statistically significant data.

Finally, we have the efficiency losses with various waveforms to consider. Each particular waveform has different reasons as to why the network efficiency will not reach 100%. For our purposes of exploring network and pipeline efficiencies and setting an upper limit on GW from CCSN, we only need efficiencies up to 90%, but there are still waveforms that do not reach this goal. For instance, if we take a look at the Yakunin High threshold efficiencies in [INSERT FIGURE], we see the efficiency is just shy of the necessary 90% value.

In Figure 6 we see the spectrogram of the injected and reconstructed signals in of an event that was injected, but not detected. We can see that this waveform has its energy greatly dispersed in the time-frequency domain. This is an issue for cWB as it uses a clustering technique to single out events. In our search, the clusters are defined by a frequency gap of 128Hz and a time gap of 0.05s. This means that lower energy clusters may not be included as part of the event. This means part of the waveform is excluded and added to the null energy making it harder for what remains of the signal to survive cuts. Compounding this problem is the fact that this waveform is linearly polarized meaning that, depending on the signal orientation, part or all of this signal could be adding to the null energy leaving less of the energy to make up the signal. The solution to this problem is quite simple. Our

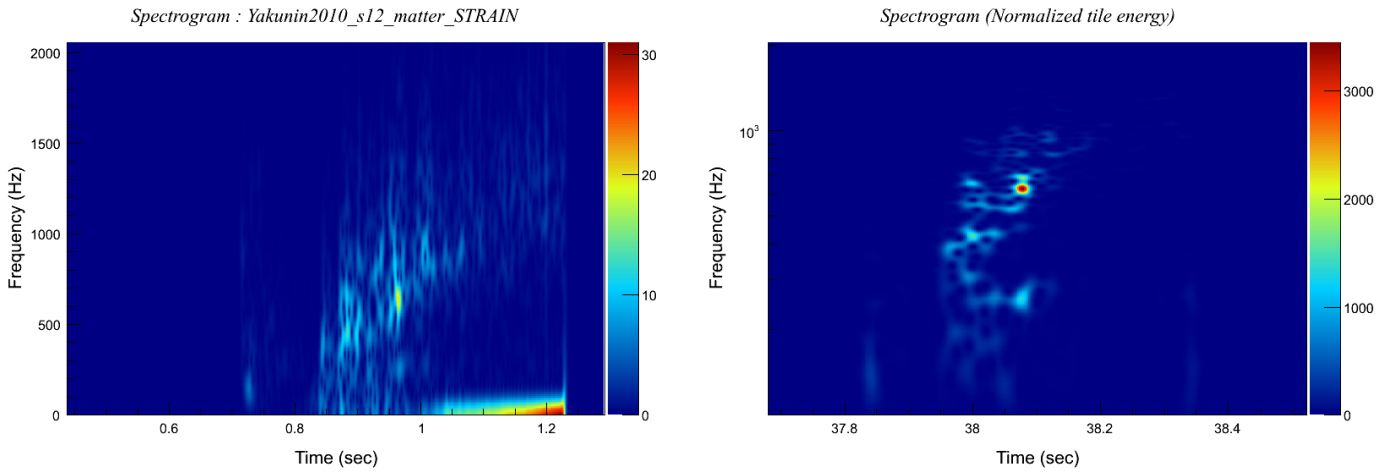

FIG. 6: Spectrogram of the Yakunin2010_s12_matter waveform before processing (Left) Spectrogram of the reconstructed signal (right) Note: Both Plots are of Normalized energy

loosened tuning with a lower ρ threshold solves this problem and boosts our efficiency above 90% without to large a loss to the false alarm rate.

Why an injected event is missed is not always so easy to solve. In the same waveform family, there is a Yakunin2010_s15_matter injection that is also missed, even with the loosened tuning cuts. Looking at a sky map of the null energy of this event, Figure 7, we see that the injected position (the white star) is just on the edge of an area of very high null energy. Because of this, the signal, which like all the members of the Yakunin waveform family is very dispersed in the time/frequency domain, is lost in the noise. There is nothing that can be done to recover this event. It is situations like this that make the standard signal loss using the cWB algorithm about 2.9% [13].

Fortunately though, for each problematic waveform family there is a nice one that requires no tinkering to get good results. The analytic waveform models generate the best results. They have the best 50 and 90% hrss values and have very few missed injections. This is largely due to the fact that they are elliptically polarized, meaning that as the angle ψ rotates, no signal portion is lost and added to the null stream. It is instead simply added to the other component. This greatly reduces the dependence on the network antenna pattern. A sample of the Fryer et al. 2002 waveform efficiencies can be seen in Figure 8.

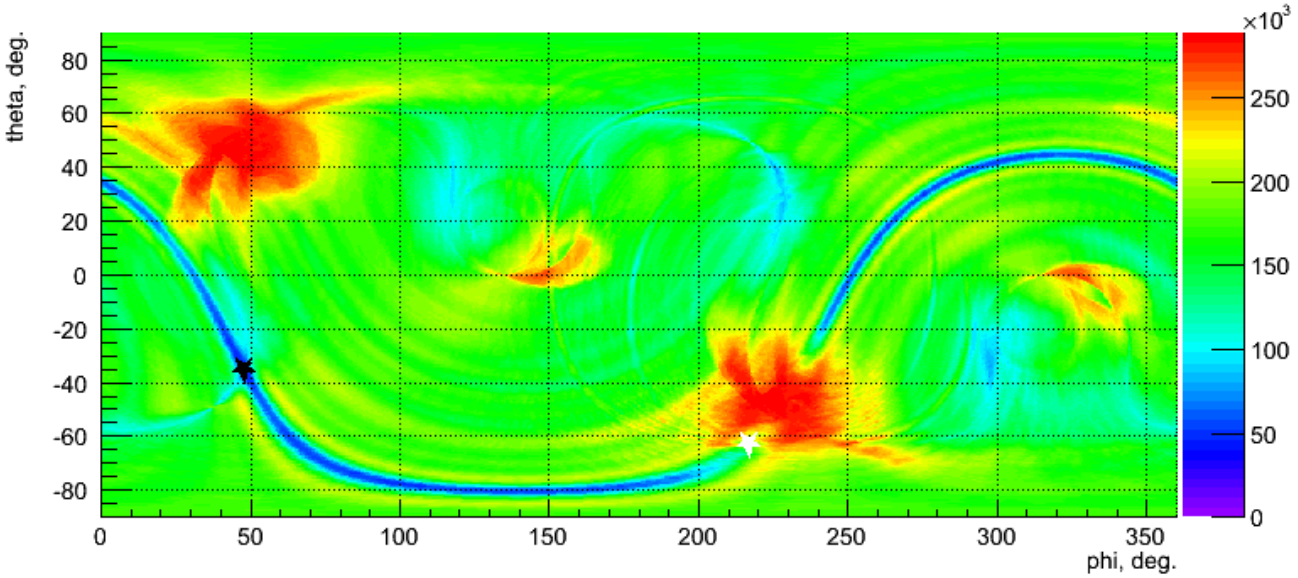

FIG. 7: Yakunin2010_s15_matter injection null energy skymap

V. CURRENT RESULTS

In Table II and Table III are the results of our most recent set of simulations implementing our skymask and our hard tuning. Several of the waveforms do not include 90% values, but instead include the efficiency at which the waveform peaks in this tuning. For the purposes of this report, it was deemed best to present the best results thus far and not intermediate tuning runs that may be more thorough. It is important to note that the waveforms which have below 90% efficiencies are all linearly polarized and will likely be fixed simply with out loosened tuning runs. The missed injections are mostly due to the portion of the waveform that contributes to the null energy. This is not a factor in the elliptically polarized signals.

VI. FURTHER WORK

We are currently in the process of performing a pipeline comparison with the parallel CalTech X-pipeline effort using the recent 2011dh supernova. This effort is using only double-coincidence triggers on S5 data. We are considering triple-coincidence triggers on

TABLE II: Numerical simulation waveforms and their results from the hard tuning

Waveform	Polarization	50% h_{rss}	90% h_{rss}
Kotake2009_Total_Equator_L676	Elliptical	1.792e-21	2.851e-21
Kotake2009_Total_Polar_L676	Elliptical	2.268e-21	3.609e-21
Kotake2009_Total_Equator_L68	Elliptical	3.005e-21	4.431e-21
Kotake2009_Total_Polar_L68	Elliptical	2.513e-21	3.609e-21
Ott2009_nomoto13	Linear	1.485e-21	89%
Ott2009_nomoto15	Linear	2.124e-21	4.273e-21
Ott2009_s11.2	Linear	1.887e-21	4.874e-21
Ott2009_s13.0	Linear	1.430e-21	6.075e-21
Ott2009_s15.0	Linear	1.616e-21	89%
Ott2009_s20.0	Linear	1.198e-21	89%
Ott2009_s25.0	Linear	1.558e-21	89%
Ott2010_u75rot15	Linear	1.527e-21	89%
Ott2010_u75rot1	Linear	1.502e-21	89%
Ott2010_u75rot2	Linear	1.434e-21	89%
Marek2009_matter_ls	Linear	2.288e-21	89%
Marek2009_matter_wolff	Linear	8.871e-22	1.902e-21
Scheidegger2010_R0STCA	Elliptical	6.316e-22	9.536e-22
Scheidegger2010_R0E1CA	Elliptical	5.897e-22	9.220e-22
Scheidegger2010_R0E3CA	Elliptical	7.105e-22	1.080e-21
Scheidegger2010_R1E1CA	Elliptical	6.562e-22	8.588e-22
Scheidegger2010_R1E1CA_L	Elliptical	8.884e-22	1.459e-21
Scheidegger2010_R1E1DB	Elliptical	6.758e-22	1.143e-21
Scheidegger2010_R1E3CA	Elliptical	6.827e-22	9.536e-22
Scheidegger2010_R1STCA	Elliptical	5.815e-22	1.112e-21
Scheidegger2010_R2E1AC	Elliptical	1.279e-21	1.902e-21
Yakunin2010_s12_matter	Linear	2.651e-21	89%
Yakunin2010_s15_matter	Linear	4.227e-21	89%
Yakunin2010_s25_matter	Linear	6.025e-21	89%

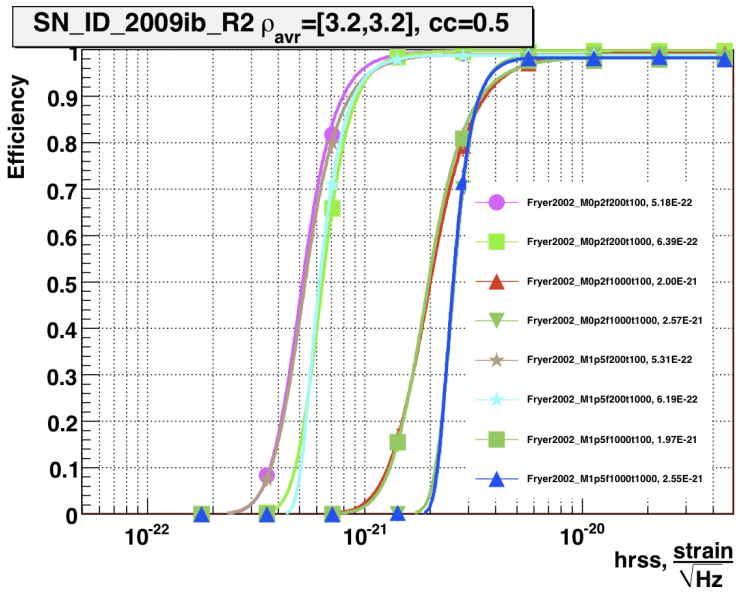

FIG. 8: The efficiency curve for the analytic Fryer2002 waveforms. The analytic waveforms are interesting because the roughly model physical events while providing comparisons for detector sensitivities as a function of parameters like frequency.

S6. This is rather difficult as the only detector data available is G1V1 data. Until recently, the G1 data had a GPS time error. Since then, we have found that the similar detector orientation of the G1V1 arms makes it impossible to use a skymask as we lose 50% of our injected signals. As such, we must use an all sky search and apply a similar improvement that we see in the L1H1V1 data when comparing all-sky and targeted searches.

Currently, we have only dealt with triple coincidence data. We would like to incorporate double coincidence data as well which means we will be performing the same searches using two detector permutations of L1H1V1 detectors. After all of our simulations are completed, we will run all of these searches on the 0 lag data to see what we find. After collecting all of our results, we hope to publish a paper on either suspected detections or on upper limits of GW transients from supernovae.

For current and future status, see our working webpage:

`http://mercury.pr.erau.edu/~corpuza/waveforms/page.html`

TABLE III: Analytic waveform results from the hard tuning

Waveform	Polarization	50% h_{rss}	90% h_{rss}
Fryer2002_M0p2f200t100	Elliptical	5.175e-22	7.956e-22
Fryer2002_M0p2f200t1000	Elliptical	6.386E-22	9.220e-22
Fryer2002_M0p2f1000t100	Elliptical	2.005e-21	3.609e-21
Fryer2002_M0p2f1000t1000	Elliptical	2.574e-21	3.388e-21
Fryer2002_M1p5f200t100	Elliptical	5.315e-22	8.588e-22
Fryer2002_M1p5f200t1000	Elliptical	6.186e-22	8.904e-22
Fryer2002_M1p5f1000t100	Elliptical	1.966e-21	3.451e-21
Fryer2002_M1p5f1000t1000	Elliptical	2.551e-21	3.388e-21
Piro2007_M5eta0p3	Elliptical	1.098e-21	1.681e-21
Piro2007_M5eta0p5	Elliptical	8.464e-22	1.301e-21
Piro2007_M7eta0p3	Elliptical	9.786e-22	1.523e-21
Piro2007_M7eta0p5	Elliptical	9.662e-22	1.523e-21
Piro2007_M10eta0p3	Elliptical	9.604e-22	1.491e-21
Piro2007_M10eta0p5	Elliptical	9.250e-22	1.459e-21
Piro2007_M15eta0p3	Elliptical	9.034e-22	1.428e-21
Piro2007_M15eta0p5	Elliptical	8.868e-22	1.333e-21
Piro2007_M20eta0p3	Elliptical	8.092e-22	1.207e-21
Piro2007_M20eta0p5	Elliptical	8.467e-22	1.270e-21

VII. CONCLUSIONS

As this project is ongoing, it is hard to make any conclusive statements. Over this two month working period, we have gained a much greater understanding of the waveforms we are using and their own particular characteristics. We have managed to improve our detector efficiencies for each waveform by a minimum factor of two. Our search has matured significantly enough that we are now able to consider a comparison with the CalTech X-pipeline search. Our preliminary reach estimates put the effective detection range of some

of our analytic models out to a few megaparsecs.

---

[1] http://gwic.ligo.org/roadmap/Roadmap_100814.pdf

[2] C. D Ott. TOPICAL REVIEW: The gravitational-wave signature of core-collapse supernovae. Classical and Quantum Gravity, 26(6):063001-+,March 2009.

[3] C. D. Ott, "Probing the Core-Collapse Supernova Mechanism with Gravitational Waves ". Class. Quant. Grav. 26, 204015, 2009

[4] A. Marek, H.-T. Janka, and E. Muller. Equation-of-state dependent features in shock-oscillation modulated neutrino and gravitational-wave signals from supernovae. A&A, 496:475-494,March 2009.

[5] K. Kotake, W. Iwakami, N. Ohnishi, and S. Yamada. Stochastic Nature of Gravitational Waves from Supernova Explosions with Standing Accretion Shock Instability. ApJ, 697:L133-L136, June 2009.

[6] S. Scheidegger, S.C. Whitehouse, R. Kappeli, and M. Liebendorfer. Gravitational waves from supernova matter. arXiv:0912.1455v2 [astro-ph.HE]

[7] K. Yakunin, P. Marronetti, A Mezzacappa, S Bruenn, C.-T. Lee, M Chertkow, W Hix, J Blondin, E Lentz, O. Messer, and S Yoshida. Gravitational Waves from Core Collapse Supernovae. arXiv:1005.0779v2. 2010

[8] C.L. Fryer, D.E. Holz, and S.A. Hughes. Astrophys. J., 565, 430, 2002.

[9] A. Piro and E. Pfahl. Fragmentation of Collapsar Disks and the Production of Gravitational Waves. ApJ, 658:1173-1176, 2007 April 1

[10] M. Drago. Search For Transient Gravitational Wave Signals With Unknown Waveform In The Ligo Virgo Network Of Inteferometric Detectors Using A Fully Coherent Algorithm. Doctoral Thesis.

[11] K. Kaufman, https://svn.ligo.caltech.edu/svn/snsearch/papers/surf_report2010/kkaufman_SURF2010.pdf

[12] A. L. Stuver, K. Thorne. LIGO-T040020-03-Z

[13] I. S. Heng, I. Ferrante, M. Zanolin. S6/VSR2 coherent Waveburst Review Report. LIGO-T1000241-x0. 2011/01/21

TABLE IV: Analytic waveform results from the hard tuning

Supernova	Host Galaxy	Date	Type	Distance (Mpc)	Position
2010K	SDSS J120246.67+022405	20100108			
2010gi	IC 4660	20100718			
2010br	NGC 4051	20100410			
2009mk	ESO 293-34	20091215			
2009md	NGC 3389	20091204			
2009ls	NGC 3423	20091123			
2009kr	NGC 1832	20091106			
2009js	NGC 0918	20091011			
2009ip	NGC 7259	20090926			
2009ib	NGC 1559	20090806			
2009hq	NGC 4152	20090730			